PERGAMON

International Journal of Heat and Mass Transfer 44 (2001) 3135–3145

International Journal of HEAT and MASS TRANSFER

www.elsevier.com/locate/ijhmt

Microscale permeability predictions of porous fibrous media

N.D. Ngo, K.K. Tamma *

Department of Mechanical Engineering, University of Minnesota, 111 Church Street SE., Minneapolis, MN 55455-0111, USA

Received 17 August 1999; received in revised form 9 October 2000

Abstract

A good understanding of woven fiber preform permeabilities is critical in the design and optimization of the composite molding processes encountered in resin transfer molding (RTM); yet these issues remain unresolved in the literature. Many have attempted to address permeability predictions for flat undeformed fiber preform, but few have investigated permeability variations for complex geometries of porous fibrous media. In this study, the objectives are to: (i) provide a brief review of existing methods for the prediction of the fiber mat permeability; (ii) postulate a more realistic representation of a unit cell to account for such fabric structures as crimp, tow spacing and the like; and (iii) apply computational approximations to predict effective permeabilities for use in modeling of structural composites manufacturing processes. The Stokes equation is used to model the flow in the inter-tow region of the unit cell, and in the intra-tow region, the Brinkman's equation is used. Initial permeability calculations are performed for a three-dimensional unit cell model representative of the PET-61 woven fabric composite. The results show good agreement with experimental data published in the literature. © 2001 Published by Elsevier Science Ltd.

1. Introduction

A common thread linking both the isothermal and non-isothermal modeling of the resin transfer molding (RTM) process in the manufacture of composites is the use of Darcy's law to describe the flow of a resin fluid through a fiber preform. As given by the Darcy's equation [1],

$$\boldsymbol{u} = -\frac{\bar{\boldsymbol{K}}}{\mu}\nabla P \tag{1}$$

all of the complicated interaction between the fluid and the fiber preform structure is lumped into the permeability tensor $\bar{\boldsymbol{K}}$, and accurate permeability data are therefore a critical requirement in the design and optimization of the RTM process. Traditionally, determination of the permeability tensor is best accomplished through experimental measurements since for the most part, various measurement techniques all yield consistent results [2]. However, these measurements often require a large number of carefully controlled experiments and, in general, have no predictive capability (i.e., each new material must be handled on a case-by-case basis). As a consequence, the ability to analytically (for simple cases) or numerically predict the permeability of the fiber preform has for the past few years been the goal of many researchers in the field of porous media flow. In this paper, a literature review of early and current efforts for predicting permeability is first presented. Then, the governing equations and formulations pertinent in the development of the present methodology are outlined. Finally, an illustrative unit cell representative of a PET-61 woven fabric composite is posed and the effective permeabilities are predicted.

2. Early and current developments

The earliest recognized investigator of fluid flow through isotropic porous media is Darcy [1], who proposed after making heuristic observations from a packed column experiment the following relation:

$$u = -\frac{k}{\mu}\frac{\partial P}{\partial x}. \tag{2}$$

* Corresponding author. Tel.: +612-625-1821; fax: +612-624-1398.

E-mail address: ktamma@tc.umn.edu (K.K. Tamma).

0017-9310/01/$ - see front matter © 2001 Published by Elsevier Science Ltd.
PII: S0017-9310(00)00335-5

Nomenclature

$\boldsymbol{B}$	spatial derivatives of shape functions
c, C_1	permeability model constants
$\boldsymbol{D}_i$	defined viscosity tensor
h_e	element characteristic length
k, K_{ij}	permeability values
$K_\parallel$	flow-direction permeability
$K_\perp$	cross-flow permeability
$\bar{\boldsymbol{K}}$, $\bar{\boldsymbol{K}}_L$, $\bar{\boldsymbol{K}}_G$	permeability tensors
K^*_{ij}	coefficients of $\bar{\boldsymbol{K}}^*$ tensor
$\bar{\boldsymbol{K}}^*$	inverse of permeability tensor (e.g., $\bar{\boldsymbol{K}}^* = \bar{\boldsymbol{K}}^{-1}$)
N_i, $\boldsymbol{N}$	finite element shape functions
P, $\boldsymbol{P}$	pressure
R	filament radius
$\boldsymbol{R}$	transformation matrix
Re	global Reynolds number ($Re = \rho/\mu(\lvert\boldsymbol{u}_G\rvert h_e/2)$)
S_0	specific surface exposed to the fluid per unit volume of solid material
t_i	traction boundary condition
u, v, w	velocity components
$\boldsymbol{u}$	velocity vector
$\boldsymbol{u}_G$	global velocity vector
$\boldsymbol{u}$, $\boldsymbol{v}$, $\boldsymbol{w}$	velocity arrays; $(u_1, u_2, \ldots, u_n)$, $(v_1, v_2, \ldots, v_n)$ and $(w_1, w_2, \ldots, w_n)$
V_f	fiber volume fraction

Greek symbols

Γ_i	boundary of domain
Ω	domain
ϕ	porosity
Φ	effective porosity of unit cell
ρ	density
$\vec{\boldsymbol{\Pi}}_L$, $\vec{\boldsymbol{\Pi}}_G$	basis vectors
μ	viscosity

In 1927, Kozeny [3] theorized that a porous medium can be represented by an assemblage of channels of various cross-sections that are of a specific length. Permeability can therefore be described in terms of a hydraulic radius and other mathematical models soon followed, drawing upon Kozeny's idea of using channels to approximate the porous medium. Unlike Darcy's law for isotropic porous media, Kozeny's work recognized the pore structure as having definite details which could be replaced mathematically with a simplified geometry.

The next significant development in the understanding of porous media flow occurred when Carman presented what is now well known as the Kozeny–Carman equation [4]

$$k = \frac{\phi^3}{5S_0^2(1-\phi)^2}. \tag{3}$$

While some critics disagree with Carman's modification because it is incapable of reproducing Kozeny's earlier calculations [5], Carman claimed that the new equation better agrees with experimental results than Kozeny's original equation [4]. In 1947, Brinkman [6] proposed a more realistic porous medium flow relation,

$$\nabla P = -\frac{\mu}{k}\boldsymbol{u} + \mu\nabla^2\boldsymbol{u}. \tag{4}$$

The presence of the Laplacian operator in Eq. (4) enables the Brinkman equation to model flow around the finite porous media where a boundary exists between the open and the porous regions.

It is important to note that in the RTM process, the employed fiber preform is typically made up of woven fiber bundles, Fig. 1. Each of the fiber bundles is called a

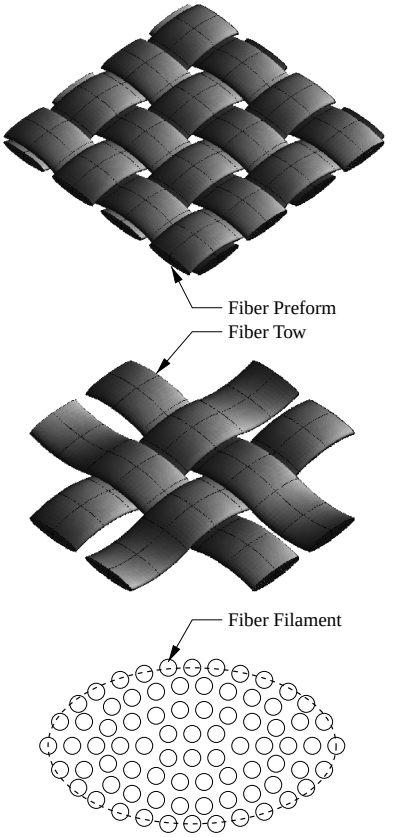

Fig. 1. Schematic of fiber preform microstructures.

tow, *fiber* or *yarn*, and each of the yarns, in turn, contains many *fibrils* or *filaments*. A collection of yarns comprises a structure known as a *fabric*, *cloth*, or a *preform mat*. Thus, at the microscopic level, flow through a fibrous porous medium is analogous to flow through banks of a heat exchanger, and it was through this analogy that researchers have sought to analytically and numerically predict the permeability of the fiber preform [2,7–11]. While the exact computational procedures vary from one researcher to another, the problem typically reduces to solving the Navier–Stokes equations and/or variations of the Navier–Stokes equations, and with Darcy's law obtaining the permeability through back substitution.

Realizing the limitations of most existing models which do not offer realistic representation of the woven fabric architecture, in a previous work at the University of Minnesota, Chung et al. [12] independently came up with the notion of using a three-dimensional unit cell for permeability predictions. As a first approximation, Chung et al. [12] and Ngo et al. [13] used Darcy's law in both the inter-tow (i.e., fluid) and intra-tow (i.e., solid) regions. In the inter-tow region, an equivalent permeability of the air gap was estimated by approximating the unit cell as a duct with a porous boundary. In the intra-tow region, permeability models based on Gebart [7] equations were used and the fibrils were assumed to pack in a hexagonal arrangement. The proposed methodology was validated and, compared with experimental results published by Adams et al. [14] for a PET-61 fabric, reasonable agreements were achieved. Chung et al. [12] attributed the difference in cross-flow permeability to the use of Darcy's law. They noted that the overall effective permeability of the unit cell was highly sensitive to the equivalent air permeability K_{air} and suggested that the Brinkman's equation may be a more appropriate model to use in the simulation.

Unlike past efforts in modeling the microstructure for determining the effective permeabilities, the present developments introduce the notion of a micro/macro unit cell from a different perspective and is based on a more realistic representation of the three-dimensional fabric architecture which includes tow crimp, spacing and the like. Two levels of microstructures are assumed and the prediction of the effective permeability values is based on first treating the individual fibril as a solid impermeable section and subsequently applying these results to a 3-D representation of a micro/macro unit cell. The overall developments, as presented in this paper, are part of a general-purpose in-house research code named On Composite Technology Of Polymeric Useful Structures (OCTOPUS) which inherits a vast finite element library, mold filling techniques, time integrators, stabilizing features, and constitutive models.

3. Governing equations

3.1. The unit cell structure

Fig. 2 depicts a representative unit cell and its corresponding microstructural levels. The first level consists of the intra-tow region where the fiber filaments are treated as arrays of solid impermeable cylinders, and the second level comprises of the micro/macro unit cell. The unit cell, in turn, is made up of the tows in a woven pattern and the fluid in the inter-tow region. In the present study, the flow in the open or fluid region of the unit cell is governed by both the continuity equation

$$\nabla \cdot \boldsymbol{u} = 0 \tag{5}$$

and the Stokes equation

$$\nabla P = \mu \nabla^2 \boldsymbol{u}. \tag{6}$$

In the intra-tow region where the tow consisted of bundles of filaments and can therefore be treated as a porous medium, the flow is modeled by the continuity equation

$$\nabla \cdot \langle \boldsymbol{u} \rangle = 0 \tag{7}$$

and the Brinkman equation which is given by

$$\nabla \langle P \rangle = \mu \nabla^2 \langle \boldsymbol{u} \rangle - \mu \bar{\boldsymbol{K}}^{-1} \cdot \langle \boldsymbol{u} \rangle. \tag{8}$$

In the remainder of this paper, the volume-averaged property of the Brinkman equation will be implicitly implied, and the velocity and pressure terms are henceforth written without the "$\langle\ \rangle$" notations.

For the case of a prescribed x direction pressure gradient as seen in Fig. 3, the boundary conditions are as follows:

- On Γ_1: $\partial u/\partial x = 0$, $v = 0$, $w = 0$ and $P = P_0$.
- On Γ_2: $\partial u/\partial x = 0$, $v = 0$, $w = 0$ and $P = 0$.
- On Γ_3 and Γ_4: $t_x = 0$, $t_y = 0$ and $w = 0$, etc. (e.g., symmetric b.c.).
- On Γ_5 and Γ_6: $t_x = 0$, $v = 0$ and $t_z = 0$, etc. (e.g., symmetric b.c.).

The use of the Brinkman equation means that the analyst is required to provide the permeability of the porous medium (e.g., the intra-tow region) as an input. For this purpose, the present developments assume that the fiber tow consists of parallel impermeable filaments arranged in a periodic pattern so that only the flow in one typical "representative cell" needs to be considered. The arrangements considered are: (i) a quadratic array, Fig. 4(a), and (ii) a hexagonal array, Fig. 4(b). The use of these arrangements, in turn, allows for the permeability models derived by Gebart [7] to be employed. For the two cases of quadratic and hexagonal arrangements of fiber filaments, the permeability equations derived by Gebart [7] are:

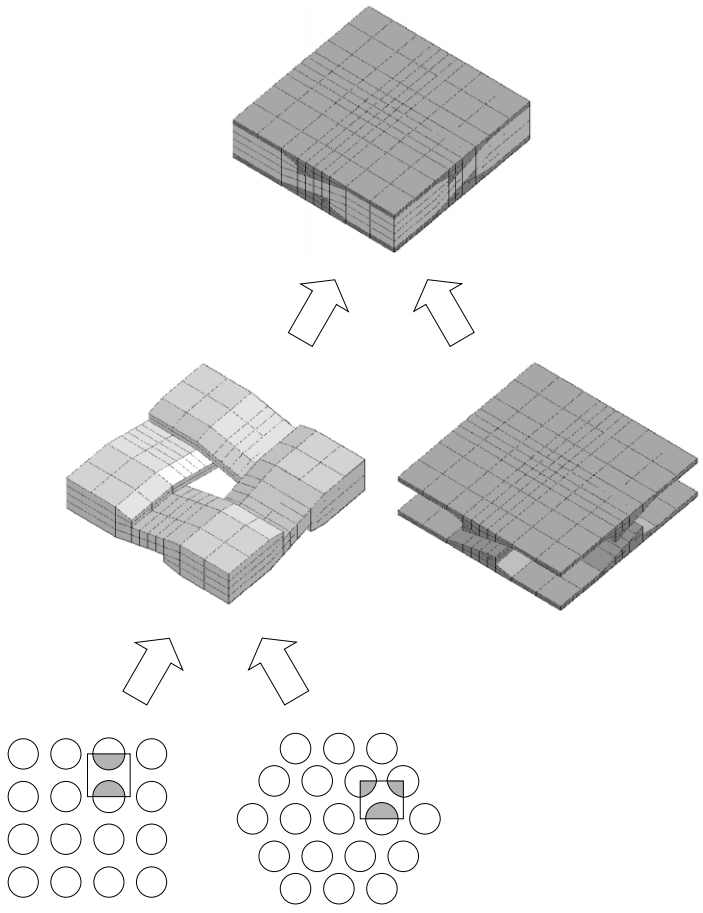

Fig. 2. Schematic diagram showing details of unit cell from microscopic to macroscopic level.

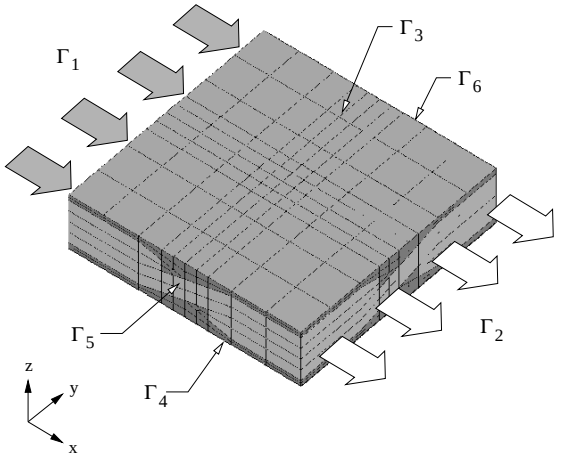

Fig. 3. Schematic diagram showing boundary conditions of unit cell.

$$K_{\parallel} = \frac{8R^2}{c}\frac{(1-V_f)^3}{V_f^2}, \tag{9}$$

$$K_{\perp} = C_1\left(\sqrt{\frac{V_{f\max}}{V_f}} - 1\right)^{5/2} R^2. \tag{10}$$

Table 1 summarizes the values of C_1, $V_{f\max}$ and c for the two types of fiber arrangements mentioned above.

3.2. Local/global transformation of permeability tensor

In the present developments, the permeability of the intra-tow region is assumed to be transversely isotropic. If the local x axis is taken to be along the direction of the fiber tow, and the local y and z axes are defined to be in the cross-tow directions as seen in Fig. 5, then the y direction permeability is equal to the z direction permeability. In terms of Gebart's [7] permeability equations, we have $K_{xx} = K_{\parallel}$ and $K_{yy} = K_{zz} = K_{\perp}$. With the off-diagonal permeability components assumed to be

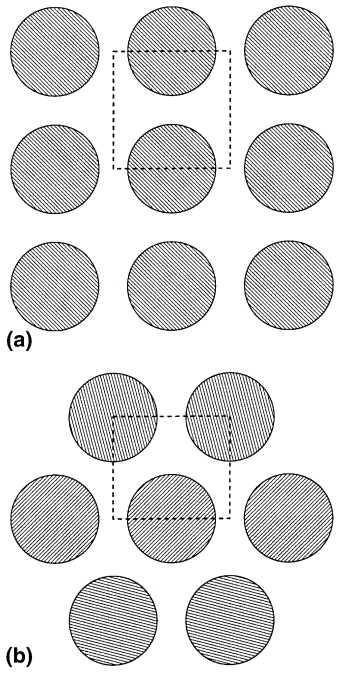

Fig. 4. Schematic of idealized intra-tow filaments and representative cell for quadratic and hexagonal fiber packing [7].

Table 1
Parameter values of permeability equations [7]

Fiber arrangement	C_1	V_{fmax}	c
Quadratic	$\frac{16}{9\pi\sqrt{2}}$	$\frac{\pi}{4}$	57
Hexagonal	$\frac{16}{9\pi\sqrt{6}}$	$\frac{\pi}{2\sqrt{3}}$	53

negligible (e.g, $K_{xy} = K_{yz} = K_{zx} \approx 0$), the local permeability tensor of the intra-tow region reduces to

$$\bar{\boldsymbol{K}}_{\mathrm{L}} = \begin{bmatrix} K_{\parallel} & 0 & 0 \\ 0 & K_{\perp} & 0 \\ 0 & 0 & K_{\perp} \end{bmatrix}. \tag{11}$$

In most situations, the local coordinates of the intra-tow region do not always align with the global coordinate of the unit cell. The undulation of the tow requires a rotation of the permeability tensor when solving for the effective permeability of the unit cell, and in the present developments, such transformation is made by using the basis vectors that define the local and the global coordinate systems of the intra-tow and the unit cell regions, respectively, Fig. 5. If both the local and the global coordinate systems are dextra-orthogonally triads, then the transformation from a *local* coordinate frame, defined by a set of basis vectors $\vec{\boldsymbol{\Pi}}_{\mathrm{L}} = (\boldsymbol{x}_{\mathrm{L}}, \boldsymbol{y}_{\mathrm{L}}, \boldsymbol{z}_{\mathrm{L}})$, to a *global* coordinate frame, defined by a set of basis vectors $\vec{\boldsymbol{\Pi}}_{\mathrm{G}} = (\boldsymbol{x}_{\mathrm{G}}, \boldsymbol{y}_{\mathrm{G}}, \boldsymbol{z}_{\mathrm{G}})$, is [15]:

$$\boldsymbol{R} = \vec{\boldsymbol{\Pi}}_{\mathrm{G}} \cdot \vec{\boldsymbol{\Pi}}_{\mathrm{L}}^{\mathrm{T}}. \tag{12}$$

In matrix form, the transformation matrix R is written as

$$\boldsymbol{R} = \begin{bmatrix} \boldsymbol{x}_{\mathrm{G}} \cdot \boldsymbol{x}_{\mathrm{L}} & \boldsymbol{x}_{\mathrm{G}} \cdot \boldsymbol{y}_{\mathrm{L}} & \boldsymbol{x}_{\mathrm{G}} \cdot \boldsymbol{z}_{\mathrm{L}} \\ \boldsymbol{y}_{\mathrm{G}} \cdot \boldsymbol{x}_{\mathrm{L}} & \boldsymbol{y}_{\mathrm{G}} \cdot \boldsymbol{y}_{\mathrm{L}} & \boldsymbol{y}_{\mathrm{G}} \cdot \boldsymbol{z}_{\mathrm{L}} \\ \boldsymbol{z}_{\mathrm{G}} \cdot \boldsymbol{x}_{\mathrm{L}} & \boldsymbol{z}_{\mathrm{G}} \cdot \boldsymbol{y}_{\mathrm{L}} & \boldsymbol{z}_{\mathrm{G}} \cdot \boldsymbol{z}_{\mathrm{L}} \end{bmatrix}. \tag{13}$$

The product of the local permeability tensor with the transformation matrices gives the global permeability tensor

$$\bar{\boldsymbol{K}}_{\mathrm{G}} = \boldsymbol{R}\,\bar{\boldsymbol{K}}_{\mathrm{L}}\,\boldsymbol{R}^{\mathrm{T}} = \begin{bmatrix} K_{11} & K_{12} & K_{13} \\ K_{21} & K_{22} & K_{23} \\ K_{31} & K_{32} & K_{33} \end{bmatrix}. \tag{14}$$

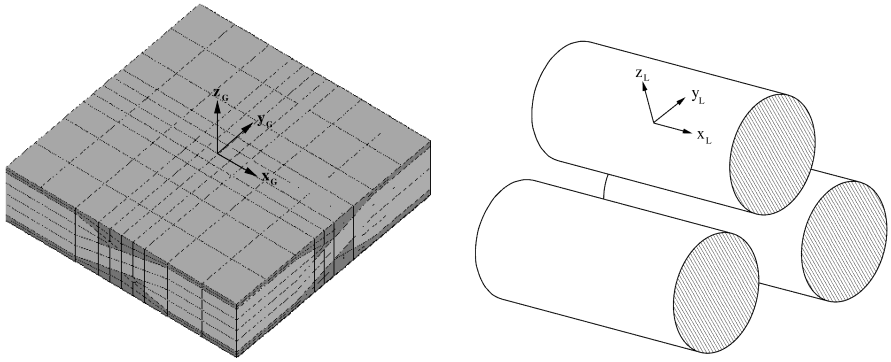

(a) Global coordinates **(b)** Local coordinates

Fig. 5. Schematic of unit cell and fiber filament showing global and local coordinate systems.

4. Finite element discretization

4.1. Momentum equation

Using the relevant components of the Stokes equation and the Brinkman equation, the momentum equation in the entire unit cell is written as

$$0 = \mu\nabla^2\boldsymbol{u} - \nabla P - \alpha\mu\bar{\boldsymbol{K}}^{-1}\cdot\boldsymbol{u}, \tag{15}$$

where α is a computational parameter that is equal to 1 in the intra-tow region and 0 in the inter-tow or open region. Thus, when α is equal to 0, Eq. (15) reduces to the Stokes equation, and when α is equal to 1, Eq. (15) is identical to the Brinkman equation. The scalar components of Eq. (15) are:

- x momentum equation:

$$0 = \left[\frac{\partial}{\partial x}\left(2\mu\frac{\partial u}{\partial x}\right) + \frac{\partial}{\partial y}\mu\left(\frac{\partial u}{\partial y}+\frac{\partial v}{\partial x}\right) + \frac{\partial}{\partial z}\mu\left(\frac{\partial u}{\partial z}+\frac{\partial w}{\partial x}\right)\right] - \frac{\partial P}{\partial x} - \alpha\mu(K^*_{11}u + K^*_{12}v + K^*_{13}w). \tag{16}$$

- y momentum equation:

$$0 = \left[\frac{\partial}{\partial x}\mu\left(\frac{\partial u}{\partial y}+\frac{\partial v}{\partial x}\right) + \frac{\partial}{\partial y}\left(2\mu\frac{\partial v}{\partial y}\right) + \frac{\partial}{\partial z}\mu\left(\frac{\partial v}{\partial z}+\frac{\partial w}{\partial y}\right)\right] - \frac{\partial P}{\partial y} - \alpha\mu(K^*_{21}u + K^*_{22}v + K^*_{23}w). \tag{17}$$

- z momentum equation:

$$0 = \left[\frac{\partial}{\partial x}\mu\left(\frac{\partial u}{\partial z}+\frac{\partial w}{\partial x}\right) + \frac{\partial}{\partial y}\mu\left(\frac{\partial v}{\partial z}+\frac{\partial w}{\partial y}\right) + \frac{\partial}{\partial z}\left(2\mu\frac{\partial w}{\partial z}\right)\right] - \frac{\partial P}{\partial z} - \alpha\mu(K^*_{31}u + K^*_{32}v + K^*_{33}w), \tag{18}$$

where K^*_{ij} are the components of the inverse of the global permeability tensor $\bar{\boldsymbol{K}}$ such that

$$\bar{\boldsymbol{K}}^* = \bar{\boldsymbol{K}}^{-1} = \begin{bmatrix} K_{11} & K_{12} & K_{13} \\ K_{21} & K_{22} & K_{23} \\ K_{31} & K_{32} & K_{33} \end{bmatrix}^{-1} = \begin{bmatrix} K^*_{11} & K^*_{12} & K^*_{13} \\ K^*_{21} & K^*_{22} & K^*_{23} \\ K^*_{31} & K^*_{32} & K^*_{33} \end{bmatrix}. \tag{19}$$

The boundary conditions of the above momentum equations are:

$$u = u_0, \quad v = v_0, \quad w = w_0 \quad \text{on} \quad \Gamma_1 \tag{20}$$

and

$$\left.\begin{aligned} t_x &= \left(-P + 2\mu\tfrac{\partial u}{\partial x}\right)n_x + \mu\left(\tfrac{\partial u}{\partial y}+\tfrac{\partial v}{\partial x}\right)n_y + \mu\left(\tfrac{\partial u}{\partial z}+\tfrac{\partial w}{\partial x}\right)n_z \\ t_y &= \mu\left(\tfrac{\partial u}{\partial y}+\tfrac{\partial v}{\partial x}\right)n_x + \left(-P + 2\mu\tfrac{\partial v}{\partial y}\right)n_y + \mu\left(\tfrac{\partial v}{\partial z}+\tfrac{\partial w}{\partial y}\right)n_z \\ t_z &= \mu\left(\tfrac{\partial u}{\partial z}+\tfrac{\partial w}{\partial x}\right)n_x + \mu\left(\tfrac{\partial v}{\partial z}+\tfrac{\partial w}{\partial y}\right)n_y + \left(-P + 2\mu\tfrac{\partial w}{\partial z}\right)n_z \end{aligned}\right\} \quad \text{on} \quad \Gamma_2 \tag{21}$$

Consider for illustration the x momentum equation. Invoking the Petrov–Galerkin weighted residual method and using equal-order shape functions for both velocity and pressure (i.e., PSPG formulations; see discussions in next section), we get

$$0 = \int_\Omega W\left[\frac{\partial}{\partial x}\left(2\mu\frac{\partial u}{\partial x}\right) + \frac{\partial}{\partial y}\mu\left(\frac{\partial u}{\partial y}+\frac{\partial v}{\partial x}\right) + \frac{\partial}{\partial z}\mu\left(\frac{\partial u}{\partial z}+\frac{\partial w}{\partial x}\right)\right]\mathrm{d}\Omega - \int_\Omega W\frac{\partial P}{\partial x}\mathrm{d}\Omega - \int_\Omega W\alpha\mu\left(K^*_{11}u + K^*_{12}v + K^*_{13}w\right)\mathrm{d}\Omega. \tag{22}$$

Using the Green–Gauss theorem on the first and second integrals in Eq. (22) and approximating the variable fields with

$$W = N_i, \quad u = N_iu_i, \quad v = N_iv_i, \quad w = N_iw_i, \quad P = N_iP_i. \tag{23}$$

Eq. (22) becomes

$$\begin{aligned} \int_\Gamma N_it_x\mathrm{d}\Gamma = &\left[\int_\Omega \frac{\partial N_i}{\partial x}2\mu\frac{\partial N_j}{\partial x}\mathrm{d}\Omega + \int_\Omega \frac{\partial N_i}{\partial y}\mu\frac{\partial N_j}{\partial y}\mathrm{d}\Omega + \int_\Omega \frac{\partial N_i}{\partial z}\mu\frac{\partial N_j}{\partial z}\mathrm{d}\Omega + \int_\Omega N_i\alpha\mu K^*_{11}N_j\mathrm{d}\Omega\right]u_j \\ &+ \left[\int_\Omega \frac{\partial N_i}{\partial y}\mu\frac{\partial N_j}{\partial x}\mathrm{d}\Omega + \int_\Omega N_i\alpha\mu K^*_{12}N_j\mathrm{d}\Omega\right]v_j \\ &+ \left[\int_\Omega \frac{\partial N_i}{\partial z}\mu\frac{\partial N_j}{\partial x}\mathrm{d}\Omega + \int_\Omega N_i\alpha\mu K^*_{13}N_j\mathrm{d}\Omega\right]w_j \\ &- \left[\int_\Omega \frac{\partial N_i}{\partial x}N_j\mathrm{d}\Omega\right]P_j, \end{aligned} \tag{24}$$

where t_x is the traction boundary condition given in Eq. (21). Eq. (24) can also be written as

$$\begin{aligned} \int_\Gamma \boldsymbol{N}^{\mathrm{T}}t_x\mathrm{d}\Gamma = &\left[\int_\Omega \boldsymbol{B}^{\mathrm{T}}\boldsymbol{D}_x\boldsymbol{B}\mathrm{d}\Omega + \int_\Omega \boldsymbol{N}^{\mathrm{T}}\alpha\mu K^*_{11}\boldsymbol{N}\mathrm{d}\Omega\right]\boldsymbol{u} \\ &+ \left[\int_\Omega \frac{\partial\boldsymbol{N}^{\mathrm{T}}}{\partial y}\mu\frac{\partial\boldsymbol{N}}{\partial x}\mathrm{d}\Omega + \int_\Omega \boldsymbol{N}^{\mathrm{T}}\alpha\mu K^*_{12}\boldsymbol{N}\mathrm{d}\Omega\right]\boldsymbol{v} \\ &+ \left[\int_\Omega \frac{\partial\boldsymbol{N}^{\mathrm{T}}}{\partial z}\mu\frac{\partial\boldsymbol{N}}{\partial x}\mathrm{d}\Omega + \int_\Omega \boldsymbol{N}^{\mathrm{T}}\alpha\mu K^*_{13}\boldsymbol{N}\mathrm{d}\Omega\right]\boldsymbol{w} \\ &- \left[\int_\Omega \frac{\partial\boldsymbol{N}^{\mathrm{T}}}{\partial x}\boldsymbol{N}\mathrm{d}\Omega\right]\boldsymbol{P}, \end{aligned} \tag{25}$$

where $\boldsymbol{D}_x$ is the viscosity tensor defined as

$$\boldsymbol{D}_x = \begin{bmatrix} 2\mu & 0 & 0 \\ 0 & \mu & 0 \\ 0 & 0 & \mu \end{bmatrix}. \tag{26}$$

Following the same FEM procedures described above, the y momentum equation is discretized as:

$$\int_\Gamma \boldsymbol{N}^{\mathrm{T}} t_y \,\mathrm{d}\Gamma = \left[\int_\Omega \frac{\partial \boldsymbol{N}^{\mathrm{T}}}{\partial x}\mu\frac{\partial \boldsymbol{N}}{\partial y}\,\mathrm{d}\Omega + \int_\Omega \boldsymbol{N}^{\mathrm{T}}\alpha\mu K_{21}^{*}\boldsymbol{N}\,\mathrm{d}\Omega\right]\boldsymbol{u} + \left[\int_\Omega \boldsymbol{B}^{\mathrm{T}}\boldsymbol{D}_y\boldsymbol{B}\,\mathrm{d}\Omega + \int_\Omega \boldsymbol{N}^{\mathrm{T}}\alpha\mu K_{22}^{*}\boldsymbol{N}\,\mathrm{d}\Omega\right]\boldsymbol{v} + \left[\int_\Omega \frac{\partial \boldsymbol{N}^{\mathrm{T}}}{\partial z}\mu\frac{\partial \boldsymbol{N}}{\partial y}\,\mathrm{d}\Omega + \int_\Omega \boldsymbol{N}^{\mathrm{T}}\alpha\mu K_{23}^{*}\boldsymbol{N}\,\mathrm{d}\Omega\right]\boldsymbol{w} - \left[\int_\Omega \frac{\partial \boldsymbol{N}^{\mathrm{T}}}{\partial y}\boldsymbol{N}\,\mathrm{d}\Omega\right]\boldsymbol{P} \tag{27}$$

and the z momentum equation is discretized as

$$\int_\Gamma \boldsymbol{N}^{\mathrm{T}} t_z \,\mathrm{d}\Gamma = \left[\int_\Omega \frac{\partial \boldsymbol{N}^{\mathrm{T}}}{\partial x}\mu\frac{\partial \boldsymbol{N}}{\partial z}\,\mathrm{d}\Omega + \int_\Omega \boldsymbol{N}^{\mathrm{T}}\alpha\mu K_{31}^{*}\boldsymbol{N}\,\mathrm{d}\Omega\right]\boldsymbol{u} + \left[\int_\Omega \frac{\partial \boldsymbol{N}^{\mathrm{T}}}{\partial y}\mu\frac{\partial \boldsymbol{N}}{\partial z}\,\mathrm{d}\Omega + \int_\Omega \boldsymbol{N}^{\mathrm{T}}\alpha\mu K_{32}^{*}\boldsymbol{N}\,\mathrm{d}\Omega\right]\boldsymbol{v} + \left[\int_\Omega \boldsymbol{B}^{\mathrm{T}}\boldsymbol{D}_z\boldsymbol{B}\,\mathrm{d}\Omega + \int_\Omega \boldsymbol{N}^{\mathrm{T}}\alpha\mu K_{33}^{*}\boldsymbol{N}\,\mathrm{d}\Omega\right]\boldsymbol{w} - \left[\int_\Omega \frac{\partial \boldsymbol{N}^{\mathrm{T}}}{\partial z}\boldsymbol{N}\,\mathrm{d}\Omega\right]\boldsymbol{P}, \tag{28}$$

$\boldsymbol{D}_y$ and $\boldsymbol{D}_z$ in Eqs. (27) and (28) are the y and z viscosity tensors defined as

$$\boldsymbol{D}_y = \begin{bmatrix}\mu & 0 & 0\\ 0 & 2\mu & 0\\ 0 & 0 & \mu\end{bmatrix} \quad \text{and} \quad \boldsymbol{D}_z = \begin{bmatrix}\mu & 0 & 0\\ 0 & \mu & 0\\ 0 & 0 & 2\mu\end{bmatrix} \tag{29}$$

respectively.

4.2. Continuity equation and pressure stabilizing Petrov–Galerkin (PSPG) formulation

In the present developments, the continuity equation given by

$$\frac{\partial u}{\partial x}+\frac{\partial v}{\partial y}+\frac{\partial w}{\partial z}=0 \tag{30}$$

is weighted using the normal finite element shape functions. The weighted residuals of the momentum equations are then added to stabilize the pressure oscillations so that equal order interpolation function can be used on the pressure term [16]. The resulting formulations, as described by Hughes [16], are termed the Pressure Stabilizing Petrov–Galerkin (PSPG) formulation and present the discretized continuity equation as

$$\int_\Omega W\left(\frac{\partial u}{\partial x}+\frac{\partial v}{\partial y}+\frac{\partial w}{\partial z}\right)\mathrm{d}\Omega + \int_\Omega (\gamma_x R_x+\gamma_y R_y+\gamma_z R_z)\,\mathrm{d}\Omega = 0, \tag{31}$$

where

$$\gamma_x = \lambda\frac{\partial W}{\partial x}, \quad \gamma_y = \lambda\frac{\partial W}{\partial y}, \quad \gamma_z = \lambda\frac{\partial W}{\partial z} \tag{32}$$

and R_i are the residual of the momentum equations defined as

$$\begin{aligned}
R_x &= -\left[\frac{\partial}{\partial x}\left(2\mu\frac{\partial u}{\partial x}\right)+\frac{\partial}{\partial y}\mu\left(\frac{\partial u}{\partial y}+\frac{\partial v}{\partial x}\right)+\frac{\partial}{\partial z}\mu\left(\frac{\partial u}{\partial z}+\frac{\partial w}{\partial x}\right)\right] + \frac{\partial P}{\partial x}+\alpha\mu\left(K_{11}^{*}u+K_{12}^{*}v+K_{13}^{*}w\right),\\
R_y &= -\left[\frac{\partial}{\partial x}\mu\left(\frac{\partial u}{\partial y}+\frac{\partial v}{\partial x}\right)+\frac{\partial}{\partial y}\left(2\mu\frac{\partial v}{\partial y}\right)+\frac{\partial}{\partial z}\mu\left(\frac{\partial v}{\partial z}+\frac{\partial w}{\partial y}\right)\right] + \frac{\partial P}{\partial y}+\alpha\mu\left(K_{21}^{*}u+K_{22}^{*}v+K_{23}^{*}w\right),\\
R_z &= -\left[\frac{\partial}{\partial x}\mu\left(\frac{\partial u}{\partial z}+\frac{\partial w}{\partial x}\right)+\frac{\partial}{\partial y}\mu\left(\frac{\partial v}{\partial z}+\frac{\partial w}{\partial y}\right)+\frac{\partial}{\partial z}\left(2\mu\frac{\partial w}{\partial z}\right)\right] + \frac{\partial P}{\partial z}+\alpha\mu\left(K_{31}^{*}u+K_{32}^{*}v+K_{33}^{*}w\right).
\end{aligned} \tag{33}$$

Assuming that the viscous terms are negligible as could be done for linear elements [16], and substituting definitions of γ_i into Eq. (31), the PSPG formulated continuity equation is defined as

$$\begin{aligned}
0 = &\int_\Omega W\left(\frac{\partial u}{\partial x}+\frac{\partial v}{\partial y}+\frac{\partial w}{\partial z}\right)\mathrm{d}\Omega\\
&+\int_\Omega \lambda\frac{\partial W}{\partial x}\left[\frac{\partial P}{\partial x}+\alpha\mu\left(K_{11}^{*}u+K_{12}^{*}v+K_{13}^{*}w\right)\right]\mathrm{d}\Omega\\
&+\int_\Omega \lambda\frac{\partial W}{\partial y}\left[\frac{\partial P}{\partial y}+\alpha\mu\left(K_{21}^{*}u+K_{22}^{*}v+K_{23}^{*}w\right)\right]\mathrm{d}\Omega\\
&+\int_\Omega \lambda\frac{\partial W}{\partial z}\left[\frac{\partial P}{\partial z}+\alpha\mu\left(K_{31}^{*}u+K_{32}^{*}v+K_{33}^{*}w\right)\right]\mathrm{d}\Omega.
\end{aligned} \tag{34}$$

where

$$\lambda = \xi\frac{h_{\mathrm{e}}}{2|\boldsymbol{u}_{\mathrm{G}}|}, \quad \xi = \coth(Re)-\frac{1}{Re}. \tag{35}$$

Letting $W = N_i$, and approximating

$$u = N_i u_i, \quad v = N_i v_i, \quad w = N_i w_i, \quad P = N_i P_i. \tag{36}$$

Eq. (34) becomes

$$\begin{aligned}
0 = &\left[\int_\Omega \boldsymbol{N}^{\mathrm{T}}\frac{\partial \boldsymbol{N}^{\mathrm{T}}}{\partial x}\,\mathrm{d}\Omega + \int_\Omega \lambda\boldsymbol{B}^{\mathrm{T}}\alpha\mu\begin{Bmatrix}K_{11}^{*}\\ K_{21}^{*}\\ K_{31}^{*}\end{Bmatrix}\boldsymbol{N}\,\mathrm{d}\Omega\right]\boldsymbol{u}\\
&+\left[\int_\Omega \boldsymbol{N}^{\mathrm{T}}\frac{\partial \boldsymbol{N}^{\mathrm{T}}}{\partial y}\,\mathrm{d}\Omega + \int_\Omega \lambda\boldsymbol{B}^{\mathrm{T}}\alpha\mu\begin{Bmatrix}K_{12}^{*}\\ K_{22}^{*}\\ K_{32}^{*}\end{Bmatrix}\boldsymbol{N}\,\mathrm{d}\Omega\right]\boldsymbol{v}\\
&+\left[\int_\Omega \boldsymbol{N}^{\mathrm{T}}\frac{\partial \boldsymbol{N}^{\mathrm{T}}}{\partial z}\,\mathrm{d}\Omega + \int_\Omega \lambda\boldsymbol{B}^{\mathrm{T}}\alpha\mu\begin{Bmatrix}K_{13}^{*}\\ K_{23}^{*}\\ K_{33}^{*}\end{Bmatrix}\boldsymbol{N}\,\mathrm{d}\Omega\right]\boldsymbol{w}\\
&+\left[\int_\Omega \lambda\boldsymbol{B}^{\mathrm{T}}\boldsymbol{B}\right]\boldsymbol{P}.
\end{aligned} \tag{37}$$

Finally, in matrix form, we have for both the momentum and continuity equations the following system of discretized equations:

$$\begin{bmatrix} \boldsymbol{K}_{11} & \boldsymbol{K}_{12} & \boldsymbol{K}_{13} & \boldsymbol{K}_{14} \\ \boldsymbol{K}_{21} & \boldsymbol{K}_{22} & \boldsymbol{K}_{23} & \boldsymbol{K}_{24} \\ \boldsymbol{K}_{31} & \boldsymbol{K}_{32} & \boldsymbol{K}_{33} & \boldsymbol{K}_{34} \\ \boldsymbol{K}_{41} & \boldsymbol{K}_{42} & \boldsymbol{K}_{43} & \boldsymbol{K}_{44} \end{bmatrix} \begin{Bmatrix} \boldsymbol{u} \\ \boldsymbol{v} \\ \boldsymbol{w} \\ \boldsymbol{P} \end{Bmatrix} = \begin{Bmatrix} \boldsymbol{F}_x \\ \boldsymbol{F}_y \\ \boldsymbol{F}_z \\ 0 \end{Bmatrix}, \tag{38}$$

where the sub-stiffness matrices $\boldsymbol{K}_{ij}$ and the load arrays $\boldsymbol{F}_i$ are given in Eqs. (25), (27), (28) and (37) for the x, y, z momentum equations and the continuity equation, respectively.

5. Permeability prediction of PET-61 fabric

As an initial study, the permeability of a PET-61 fabric composite is predicted. As stated by Adams et al. [14], PET-61 is a plain biaxially unbalanced weave shown photographically in Fig. 6. The number of tows per inch in the machine direction is 61, while that in the cross direction is 41. The measured diameter of the PET-61 fiber filament is 23 μm and the number of filaments per tow is 50 in both directions. In the present developments, the fiber filaments are assumed to pack in a hexagonal arrangement because: (i) it is more difficult to naturally stack the filaments in a quadratic arrangement, and (ii) the filaments themselves tend to rearrange and nest upon application of a compaction force at the closing of the mold [9]. From these published data, a unit cell representative of the biaxially woven PET-61 fabric is constructed and is given in Fig. 7a. The local porosity of the tows aligned in the cross direction is estimated to be 0.2, and for the tows aligned in the machine direction, this value is 0.3. The overall or effective porosity of the unit cell is 0.47 and is defined here as

$$\Phi = 1 - \frac{\text{Total volume occupied by fibrils}}{\text{Total volume of unit cell}}. \tag{39}$$

Using Gebart's permeability equations [7], the local permeabilities of the tows oriented in the cross direction are $K_{\parallel} = 2.49 \times 10^{-9}$ cm^2 and $K_{\perp} = 3.25 \times 10^{-10}$ cm^2. For the tows aligned in the machine direction, the local permeabilities are $K_{\parallel} = 1.10 \times 10^{-8}$ cm^2 and $K_{\perp} = 2.17 \times 10^{-9}$ cm^2. Fig. 7 gives the solid model and finite element mesh of the unit cell used in the permeability prediction of PET-61 fabric. The dimensions of the representative unit cell are $0.06 \times 0.04 \times 0.015$ cm, and the finite element mesh contains 2415 nodes and 1904 hexahedral elements. To be consistent with the experimental procedures, a prescribed pressure gradient is used to drive the flow; symmetric boundary conditions are imposed on the remaining unit cell surfaces. In the present developments, a prescribed pressure gradient of 1 Pa/cm is first applied in the x direction. The pressure and velocity values are then iteratively solved and once convergence is reached, the effective x direction permeability is computed through back substitution of Darcy's law:

$$\langle u \rangle = -\frac{1}{\mu} K_{xx} \left\langle \frac{\partial P}{\partial x} \right\rangle. \tag{40}$$

The y direction permeability can similarly be obtained by first imposing a pressure gradient in the y direction. Then, using the converged pressure and velocity fields,

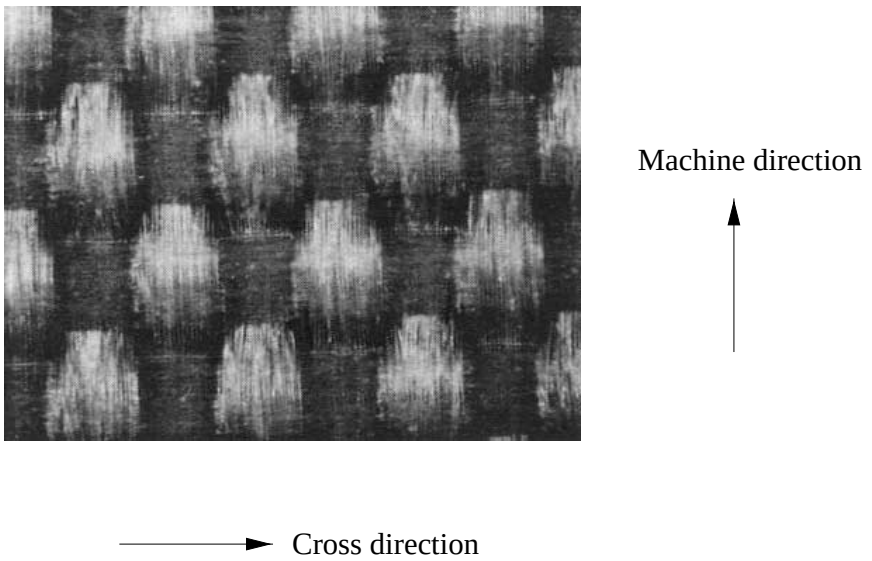

Fig. 6. Photographic view of biaxially woven PET-61 fabric [14].

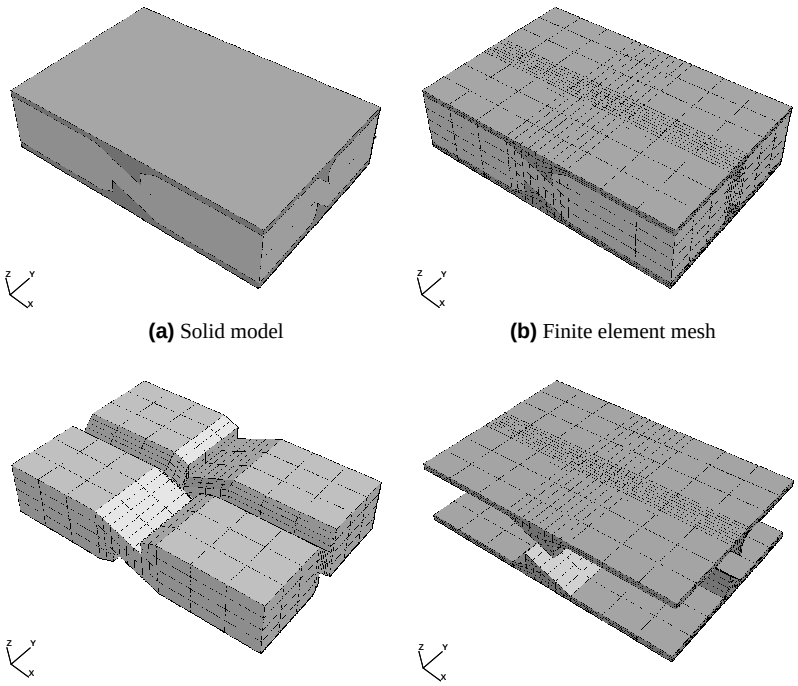

(a) Solid model **(b)** Finite element mesh

(c) Solid region **(d)** Fluid region

Fig. 7. Solid model and finite element mesh of unit cell.

the effective permeability is computed through back substitution of Darcy's law:

$$\langle v \rangle = -\frac{1}{\mu} K_{yy} \left\langle \frac{\partial P}{\partial y} \right\rangle. \tag{41}$$

Since Adams et al. [14] did not describe the specific resin used in their experiments, a viscosity value typical of many polymeric resins used in RTM at room temperature (i.e., 0.1 Pa s) was used. The pressure contours of the flow in the x and y directions are given in Figs. 8(a) and 8(b), respectively. From the converged results of the pressure and velocity fields, the effective permeabilities of the PET-61 unit cell are computed to be $K_{xx} = 2.80 \times 10^{-7}$ cm^2 and $K_{yy} = 4.31 \times 10^{-7}$ cm^2, or 28.4 and 43.7 Darcy. [1] Compared to the experimental data of $K_{xx} = 25$ and $K_{yy} = 40$ Darcy for the PET-61 fabric as published by Adams et al. [14], the results obtained by the present developments are very encouraging. The discrepancies between the two sets of results can perhaps be attributed to any of the following factors:

- Slight inaccuracy in the unit cell microstructure dimensions: It was found during the simulations that the results are very sensitive to the overall unit cell dimensions and that the open or inter-tow region alone is largely responsible for the effective permeability values. Compared to the published porosity value of 0.415, the current unit cell's effective porosity of 0.47 means that there is more room in both the intra-tow and inter-tow regions for the fluid to flow through. As a result, there is less resistance to the flow of the fluid, and permeability, which is a measure of the easiness of the flow through a porous medium, is higher – as was predicted by the present developments.
- Assumption of a hexagonal packing and the use of Gebart's permeability equations in the intra-tow region: The filaments in the actual experiments may or may not nest in this configuration so it is inevitable that differences between the computed intra-tow permeability and the experimentally obtained value will occur. Nevertheless, since Phelan and Wise [8] report from comparisons of their own experiments with permeability relations derived by Gebart [7] that the computed permeabilities appear to bound the experimental values, the choice of Gebart's models in the present developments is not totally unjustified.

It is worth nothing that in the present developments, other values of pressure gradient ranging from −1 to −10 Pa/cm and viscosity values ranging 0.01–1.0 Pa s were also used. The results obtained from these different pressure/viscosity combinations, in all cases, differ by no more than 3% from the predicted permeabilities of 28.4

[1] 1 Darcy $= 9.87 \times 10^{-9}$ cm^2 [5].

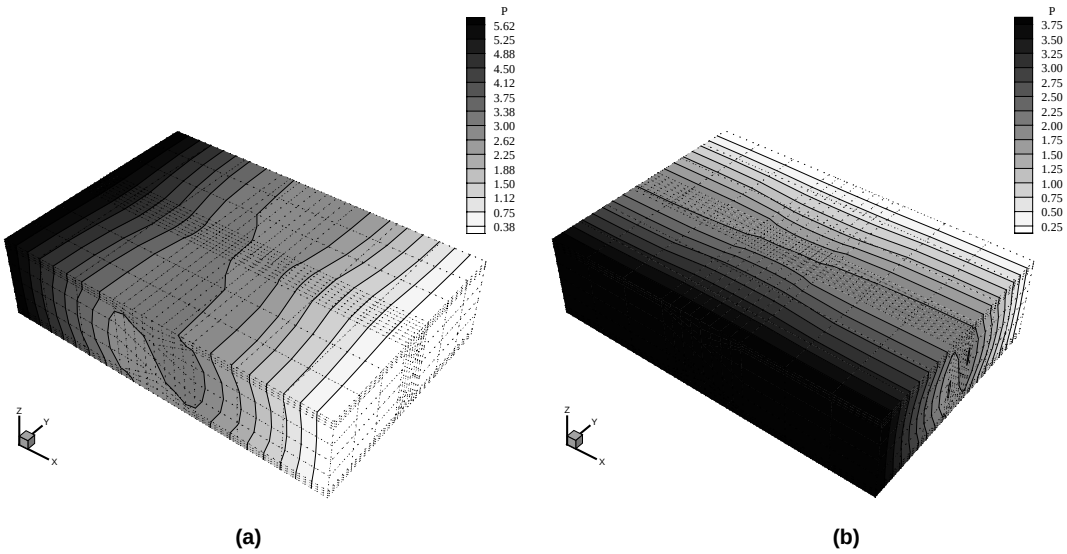

Fig. 8. Pressure contours of PET-61 unit cell.

and 43.7 Darcy. The authors believe that these differences are due more to the round-off errors associated with the large difference in magnitude (often by several orders) between the coefficients of the Stokes equation and those of the Brinkman equation (which are due to the Darcy's like term) in the system of equations than to the different pressure/viscosity values. This finding is in agreement with the theoretical belief that permeability should only be a function of the unit cell's structural properties (e.g., weave pattern, inter-tow spacing, intra-tow porosity, etc.) and should, therefore, be independent of the pressure gradient and the viscosity values.

As a final remark, since the fluid is considered to occupy the entire unit cell, the results presented by the present developments are valid only for prediction of permeability in fully saturated systems. The effective permeability in the z direction is not computed because Adams et al. [14] reported no detectable flow in the transverse direction of the PET-61 fiber mat.

6. Concluding remarks

Most current microscopic methods face limitations in their inapplicability to predict permeability in realistic complex fabric geometries and structural shapes. Their implicit assumptions require a uniform repeating structure comprising aligned tows or fibrils and unfortunately, in true fabrics, each tow encounters crimp and the assumption of aligned cylinders does not always apply. Therefore, while much progress has been made in the study of permeability prediction, many of the models proposed in the literature today [7,9–11,2,8] are only applicable to composites consisting of unidirectional fibers.

The present study, unlike past efforts in modeling the microstructure for determining the effective permeabilities, introduced the notion of a micro/macro unit from a different perspective. It is based on a more realistic representation of the three-dimensional fabric architecture and assumes, in particular, two levels of microstructures: (i) treatment of the individual fibril as a solid impermeable section, and (ii) subsequent application of these results to a 3-D representation of a micro/macro unit cell for predicting effective permeabilities.

In the present developments, the concept of using a three-dimensional unit cell to predict permeability is proposed. The flow in the open or fluid region of the unit cell is governed by the continuity equation and the creeping motion Stokes equation. In the intra-tow region where the tow consists of bundles of filaments and can therefore be treated as a porous medium, the flow is modeled by the continuity equation and the Brinkman equation. The applied boundary conditions are: (i) constant pressure gradient across two opposing surfaces to drive the flow, and (ii) symmetric conditions of pressure and velocity on the remaining surfaces of the unit cell. In the intra-tow region, the permeability of the porous medium (i.e., fiber tow) is modeled by the equations derived by Gebart [7]. These are given in terms of the axial $K_{\parallel}$ and cross flow $K_{\perp}$ permeabilities and are valid for both quadratic and hexagonal filament arrangements. The undulation of the tow through the unit cell requires that a rotation of the permeability tensor be provided when solving for the effective permeability of the unit cell.

From the modeling of a unit cell based on the data provided by Adams et al. [14], the permeabilities of PET-61 multifilament biaxial fabric were computed to be 28.4 and 43.7 Darcy for K_{xx} and K_{yy}, respectively. Compared to the experimentally measured values of 25 and 40 Darcy, the results predicted by the present developments are indeed very encouraging. Since various factors such as difficulty in obtaining exact dimensions of unit cell, slightly higher overall porosity value (0.47 versus published value of 0.415), filament nesting configuration and the like, all have some effect on the overall predicted permeability values, future efforts need to account for and will be made to more accurately describe the physics and mechanics of the representative unit cell.

Acknowledgements

The authors are very pleased to acknowledge support in part by Battelle/US Army Research Office (ARO) Research Triangle Park, North Carolina, under grant number DAAH04-96-C-0086, and by the Army High Performance Computing Research Center (AHPCRC) under the auspices of the Department of the Army, Army Research Laboratory (ARL) cooperative agreement number DAAH04-95-2-0003/contract number DAAH04-95-C-0008. The content does not necessarily reflect the position or the policy of the government, and no official endorsement should be inferred. Support in part by Dr. Andrew Mark of the Integrated Modeling and Testing (IMT) Computational Technical Activity and the ARL/MSRC facilities is also gratefully acknowledged. Special thanks are due to the CICC Directorate and the Materials Division at the US Army Research Laboratory (ARL), Aberdeen Proving Ground, Maryland. Other related support in the form of computer grants from the Minnesota Supercomputer Institute (MSI), Minneapolis, Minnesota is also gratefully acknowledged.

References

[1] H. Darcy, Les Fontaines Publiques de la Ville de Dijon, Delmont, Paris, 1856.

[2] F.R. Phelan, Y. Leung, R.S. Parnas, Modeling of microscale flow in unidirectional fibrous porous media, J. Thermoplastic Compos. Mater. 7 (1994) 208–218.

[3] J. Kozeny, Uber kapillare leitung des vassers im boden, Sitz. Akad. Wissensh. 136 (1927) 271–306.

[4] P.C. Carman, Flow of Gases Through Porous Media, Butterworths, London, 1956.

[5] A.D. Scheidegger, The Physics of Flow Through Porous Media, MacMillan, New York, 1957.

[6] H.C. Brinkman, A calculation of the viscous force exerted by a flowing fluid on a dense swarm of particles, Appl. Sci. Res. A1 (1947) 27–34.

[7] B.R. Gebart, Permeability of unidirectional reinforcements for RTM, J. Compos. Mater. 26 (8) (1992) 1100–1133.

[8] F.R. Phelan, G. Wise, Analysis of transverse flow in aligned fibrous porous media, Compos. Part A 27A (1) (1996) 25–34.

[9] S. Ranganathan, F.R. Phelan, S.G. Advani, Microstructure-permeability predictions for the processing of advanced composites, in: Annual Technical Conference – ANTEC '95, Society of Plastics Engineers, Brookfield, CT, 1995, pp. 3035–3039.

[10] K.M. Pillai, S.G. Advani, Numerical and analytical study to estimate the effect of two length scales upon the permeability of a fibrous porous medium, Transp. Porous Media (1995) 1–17.

[11] P. Simacek, S.G. Advani, Permeability model for a woven fabric, Polym. Compos. 17 (6) (1996) 887–899.

[12] P.W. Chung, N.D. Ngo, K.K. Tamma, Permeability approximations and process modeling of geometrically complex composite structures manufactured by resin transfer molding, in: AIAA-97-0140, 35th Aerospace Sciences Meeting and Exhibit, Reno, NV, January 1997.

[13] N.D. Ngo, R.V. Mohan, P.W. Chung, K.K. Tamma, Recent developments encompassing non-isothermal/isothermal liquid composite molding process modeling/analysis: physically accurate, computationally effective and affordable simulations and validations, J. Thermoplastic Compos. Mater. 11 (6) (1998) 493–532.

[14] K.L. Adams, B. Miller, L. Rebenfeld, Forced in-plane flow of an epoxy resin in fibrous networks, Polym. Eng. Sci. 26 (20) (1986) 1434–1441.

[15] P.C. Hughes, Spacecraft Attitude Dynamics, Wiley, New York, 1986.

[16] T.J.R. Hughes, L.P. Franca, M. Balestra, A new finite element formulation for computational fluid dynamics: V. Circumventing the Babuska–Brezzi condition: a stable Petrov–Galerkin formulation of the Stokes problem accomodating equal-order interpolations, Comp. Meth. Appl. Mech. Eng. 59 (1986) 85–99.